ADVANCES IN ATMOSPHERIC SCIENCES, 2025

• **Original Paper** •

A New Method to Calculate Nonlinear Optimal Perturbations for Ensemble Forecasting

Junjie MA[1], Wansuo DUAN[*2], Zhuomin LIU[3], and Ye WANG[4]

[1]*School of Mathematics*, *North University of China*, *Taiyuan* 030051, *China*
[2]*National Key Laboratory of Earth System Numerical Modeling and Application*, *Institute of Atmospheric Physics*, *Chinese Academy of Sciences*, *Beijing* 100029, *China*
[3]*School of Systems Science*, *Beijing Normal University*, *Beijing* 100091, *China*
[4]*School of Mathematics and Statistics*, *Henan University*, *Kaifeng* 475004, *China*

(Received 21 February 2024; revised 10 June 2024; accepted 8 July 2024)

ABSTRACT

Orthogonal conditional nonlinear optimal perturbations (O-CNOPs) have been used to generate ensemble forecasting members for achieving high forecasting skill of high-impact weather and climate events. However, highly efficient calculations for O-CNOPs are still challenging in the field of ensemble forecasting. In this study, we combine a gradient-based iterative idea with the Gram–Schmidt orthogonalization, and propose an iterative optimization method to compute O-CNOPs. This method is different from the original sequential optimization method, and allows parallel computations of O-CNOPs, thus saving a large amount of computational time. We evaluate this method by using the Lorenz-96 model on the basis of the ensemble forecasting ability achieved and on the time consumed for computing O-CNOPs. The results demonstrate that the parallel iterative method causes O-CNOPs to yield reliable ensemble members and to achieve ensemble forecasting skills similar to or even slightly higher than those produced by the sequential method. Moreover, the parallel method significantly reduces the computational time for O-CNOPs. Therefore, the parallel iterative method provides a highly effective and efficient approach for calculating O-CNOPs for ensemble forecasts. Expectedly, it can play an important role in the application of the O-CNOPs to realistic ensemble forecasts for high-impact weather and climate events.

Key words: initial uncertainty, conditional nonlinear optimal perturbation, optimization method, ensemble forecasting

Citation: Ma, J. J., W. S. Duan, Z. M. Liu, and Y. Wang, 2025: A new method to calculate nonlinear optimal perturbations for ensemble forecasting. *Adv. Atmos. Sci.*, https://doi.org/10.1007/s00376-024-4069-y.

Article Highlights:

- A parallel optimization method is proposed for highly efficient calculations of O-CNOPs in ensemble forecasting.
- The method greatly increases the applicability of O-CNOPs in practical ensemble forecasting.
- The O-CNOPs obtained by the new method provide reliable ensemble members with high efficiency.
- Ensemble forecasting skills as high as those generated by the original method can be achieved.

1. Introduction

In numerical weather prediction, errors are inherent due to inaccurate initial conditions and deficient models. Relevant atmospheric dynamical systems, because of their highly nonlinear and unstable nature, can quickly amplify these errors and produce significant forecast errors (Lorenz, 1963; Toth and Kalnay, 1993; Mu et al., 2003; Buizza et al., 2005; Yoden, 2007; Duan and Zhou, 2013). Ensemble forecasting is a widely used method for quantifying forecast errors. When model errors are sufficiently small and even negligible, ensemble forecasting can be treated as an initial value problem. In this situation, the distribution of the predicted states can be estimated by integrating a numerical model with uncorrelated initial perturbations (Leith, 1974), and the forecast uncertainties can be evaluated by using the statistics of these predicted states. The earliest method for producing initial perturbations for ensemble forecasts is the Monte Carlo forecasting (MCF) method, which superimposes random initial perturbations on the initial analysis field to predict the probability distribution of the forecasting results (Epstein, 1969; Leith, 1974). Subsequently, Toth and Kalnay (1993, 1997) introduced breeding vectors (BVs) for generating initial perturbations, and they emphasized that ensemble forecasts benefit from the use of growing-type ini-

* Corresponding author: Wansuo DUAN
Email: duanws@lasg.iap.ac.cn

tial perturbations. Another method for generating growing-type perturbations is the singular vectors (SVs) method. The SVs method has been utilized at the European Centre for Medium-Range Weather Forecasts (ECMWF) to construct initial perturbations for realistic weather forecasts, and demonstrated considerable improvements of the performance (Buizza et al., 1993; Buizza and Palmer, 1995; Molteni et al., 1996). The SVs method is thus far still one of the fundamental ensemble forecasting methods of the ECMWF (see https://confluence.ecmwf.int/display/FUG/).

SVs can capture the unstable growth property of initial analysis errors in the linearized regime, but they are unable to fully describe the nonlinear nature of error growth (Anderson, 1997; Hamill et al., 2000). Mu et al. (2003) proposed the approach of conditional nonlinear optimal perturbation (CNOP), which yields initial perturbations that satisfy certain physical constraints and that induces the largest nonlinear evolution at prediction time. The CNOP is viewed as an extension of the leading SV in the nonlinear regime. CNOP has been widely used to reveal the effect of nonlinearity on the predictability of atmosphere, ocean, air quality, and related high-impact weather and climate events [Duan et al., 2004; Mu et al., 2007, 2009; Duan and Zhang, 2010; Duan et al., 2018; Jiang et al., 2022, 2024; Yang et al., 2022, 2023; also see the review of Duan et al. (2023a)]. In particular, Rivière et al. (2008) extended the CNOP to study the predictability of atmospheric moisture processes; Terwisscha van Scheltinga and Dijkstra (2008) used the CNOP to explore the predictability of oceanic double gyres. Additionally, Chen et al. (2021) adopted the CNOP to reveal the sensitive area for targeted observation associated with forecasts of southwest vortices in China. Even recently, the CNOP has been utilized to identify sensitive areas for targeted observation in typhoon forecasting and oceanic state forecasting in real field campaigns (Liu et al., 2021; Feng et al., 2022; Chan et al., 2023; Qin et al., 2023).

To account for the impact of nonlinear physical processes on ensemble forecasts, Mu and Jiang (2008), as well as Jiang and Mu (2009), substituted the leading SV with CNOP and kept the other SVs unchanged for initial perturbations of ensemble forecasts. This modification improved the forecasting capability compared to that of using pure SVs. To fully consider nonlinearities, Duan and Huo (2016) proposed the orthogonal CNOPs (O-CNOPs; also see section 2) method for generating mutually independent nonlinearly optimal initial perturbations for ensemble forecasts. This method has demonstrated superior ensemble forecasting ability when compared to that of the MCF, the SVs, and the BVs methods in typhoon track forecasting (Huo and Duan, 2019; Huo et al., 2019; Duan et al., 2023a, b; Zhang et al., 2023a). Du et al. (2018) regarded O-CNOPs as an important ensemble forecasting method and included O-CNOPs in combination with other popular methods, such as BVs, SVs, and ETKF in the Handbook of Hydrometeorological Ensemble Forecasting (Duan et al., 2019). Furthermore, O-CNOPs have been utilized in real forecasts of El Niño–Southern Oscillation events and provide real-time forecast products for operational departments, revealing good forecasting capability [see Liu et al. (2023) as well as http://cmdp.ncc-cma.net/pred/cn_cmme.php?Elem=CMME-ENSO, and https://soed.sio.org.cn/emsodm.html].

O-CNOPs perform very well in their existing ensemble forecasting applications. However, the requisite numerical computation is still a fundamental challenge. Originally, Duan and Huo (2016) had to calculate O-CNOPs by using a sequential optimization method. That is, they first calculated the leading CNOP by searching for the fastest-growing initial perturbation in the space defined by the constraint condition. Then, they obtained the second CNOP in the subspace orthogonal to the first CNOP, followed by the calculation of the third CNOP in the subspace orthogonal to the first and second CNOPs, and so on [also see Huo and Duan (2019), Huo et al. (2019) and Zhang et al. (2023a)]. Each CNOP was searched along the descending direction of the gradient of the objective function with respect to the initial perturbations by using an optimization solver named Spectral Projected Gradient 2 (SPG2; Birgin et al., 2000).

The above discussion clearly shows that O-CNOPs originally require one-to-one solving, thus consuming considerable computational time and limiting the timeliness of real-time forecasts. Therefore, developing a highly efficient computational method for O-CNOPs is urgently important. In the present study, we propose an alternative method to significantly reduce the computational time and to greatly increase the timeliness of the ensemble forecasts generated by O-CNOPs.

In section 2, a new method for calculating O-CNOPs is proposed, and in section 3 the advantages of the new method are revealed based on ensemble forecasting experiments by using the Lorenz-96 model. Then, in section 4, we mainly provide a discussion on the similarity of the O-CNOPs generated by the new and old methods. Finally, a summary is provided in section 5.

2. The new method to calculate O-CNOPs

In this section, the approach of the O-CNOPs is first briefly described and then the new method to calculate the O-CNOPs is proposed.

2.1. *The O-CNOPs approach*

Equation (1) represents a dynamical system of atmospheric and oceanic motions:

$$\begin{cases} \dfrac{\partial U}{\partial t} = F(U(x,t)) \\ U|t=0 = U_0 \end{cases}, \text{in } \Omega \times [0,T], \tag{1}$$

where $U(x,t)$ describes the evolution of an atmospheric or oceanic state at a given time, U_0 is its initial state, and F is a nonlinear differential operator. $(x,t) \in \Omega \times [0,T]$, where x and t are the space coordinate and time, respectively, and Ω and T represent a domain in $\mathbb{R}^n$ and the prediction period,

respectively. If Eq. (1) and its initial state are known, the state $U(x,t)$ at time T can be given by

$$U(x,t) = M_T(U_0)\ , \tag{2}$$

where M_T is the nonlinear propagator of Eq. (1). Assuming that the model is perfect and that the initial perturbation u_0 represents the initial error, the prediction error, denoted by u_T, can be expressed as in Eq. (3):

$$u_T = M_T(U_0+u_0) - M_T(U_0)\ . \tag{3}$$

Based on Eq. (3), the O-CNOPs can be defined as follows:

$$J\left(u_{0_j}^*\right) = \max_{u_{0_j}\in\Omega_j}\left\|M_T\left(U_0+u_{0_j}\right) - M_T(U_0)\right\|_b\ , \tag{4}$$

where

$$\Omega_j = \begin{cases} \left\{u_{0_j}\in\mathbb{R}^n \left| \left\|u_{0_j}\right\|_a \leqslant \delta\right.\right\}, j=1\ , \\ \left\{u_{0_j}\in\mathbb{R}^n \left| \left\|u_{0_j}\right\|_a \leqslant \delta, u_{0_j}\perp\Omega_k, k=1,2,\cdots,j-1\right.\right\}, j>1\ . \end{cases} \tag{5}$$

Here, u_{0_j} represents the initial perturbation in subspace $\Omega_j (j=1,2,3,\cdots)$; $\|\cdot\|_a$ and $\|\cdot\|_b$ are the norms that measure the amplitudes of the initial perturbations and their evolution at prediction time T, respectively; δ is the constraint radius that indicates the scope of the initial perturbation amplitude; the symbol "$\perp$" denotes orthogonality; and the initial perturbation $u_{0_j}^*$ is the jth CNOP. For $j=1$, the optimal initial perturbation $u_{0_1}^*$ has the largest nonlinear evolution at prediction time T in the whole phase space, which is the CNOP proposed by Mu et al. (2003), and the jth CNOP has the largest nonlinear evolution at time T in the subspace orthogonal to the first $j-1$ CNOPs. Moreover, their corresponding cost function values are ranked by $J\left(u_{0_1}^*\right) > J\left(u_{0_2}^*\right) > \cdots > J\left(u_{0_n}^*\right)$.

The O-CNOPs, as mentioned in the Introduction, are often computed by tracing the descending direction of the gradient of the cost function with respect to initial perturbations. The derivation of the gradient can be found in Duan and Huo (2016). Specifically, they provided the following formula:

$$\nabla J\left(u_{0_j}\right) = 2M_T^*\left(U_0+u_{0_j}\right)\left(M_T\left(U_0+u_{0_j}\right) - M_T(U_0)\right)\ , \tag{6}$$

where M_T^* is the adjoint model of Eq. (1). Based on this gradient, previous researchers, as discussed in the Introduction, often utilized the SPG2 solver to calculate O-CNOPs one by one.

2.2. *The new method for calculating O-CNOPs*

Barkmeijer (1996) introduced an iterative method to solve the initial perturbation that possesses much larger perturbation growth than the SV in a nonlinear model. In this method, the SV is initially substituted to calculate the gradient $M_T^*\left(U_0+u_{0_j}\right)\left(M_T\left(U_0+u_{0_j}\right) - M_T(U_0)\right)$. Then, along the direction provided by this gradient, the SV is updated at a given iterative step. After several iterative steps, a new initial perturbation can be obtained, which has a much greater growth in the nonlinear model featured by M_T. It is believed that sufficient iterative steps can approach to the nonlinear optimal perturbation, i.e., the first CNOP in O-CNOPs. From Barkmeijer (1996), it is known that the iterative method allows multiple SVs to be simultaneously optimized to obtain multiple nonlinear initial perturbations. In this situation, the relevant computations facilitate the implementation of parallel computing. This approach results in a significant reduction in computational time. Inspired by this, we extend this iterative method to compute O-CNOPs simultaneously rather than compute them sequentially.

The original iterative method cannot guarantee that the resultant nonlinear initial perturbations are mutually orthogonal after sufficient iterations, as required in O-CNOPs, although it can output them simultaneously. To overcome this limitation, we incorporate the Gram–Schmidt orthogonalization [see the review of Leon et al. (2013)] with an iterative method, and we formulate a parallel iterative method for computing O-CNOPs simultaneously. The specific steps are outlined below:

Step 1. A group of mutually independent initial perturbations, $\left\{u_{0_j}^{(k)}, j=1,2,\cdots,N\right\}$, are chosen, and a parallel operation is adopted to simultaneously compute the gradients [in Eq. (6)] for these initial perturbations, where $\left\{u_{0_i}^{(k)}\perp u_{0_j}^{(k)}, i\neq j\right\}$ and N and k denote the number of initial perturbations and the number of iterative steps, respectively. The value of N is chosen according to the given ensemble forecasting problem, and $k=0,1,2,3,\cdots$. In this context, $k=0$ indicates that the initial perturbations $\left\{u_{0_j}^{(k)}, j=1,2,\cdots,N\right\}$ are the initial guess values for O-CNOPs and $k=1,2,3,\cdots$, corresponding to the update initial perturbations in Step 2.

Step 2. The gradients in Step 1 are substituted in Eq. (7), and a group of updated initial perturbations $\left\{u_{0_j}^{(k)}, j=1,2,\cdots,N\right\}$ are derived, which is inspired by the approach as proposed in Barkmeijer (1996):

$$u_{0_j}^{(k)} = u_{0_j}^{(k-1)} + \frac{\alpha}{\left\|\nabla J\left(u_{0_j}^{(k-1)}\right)\right\|}\nabla J\left(u_{0_j}^{(k-1)}\right)\ , \tag{7}$$

where ∇J is the gradient in Eq. (6), $\|\cdot\|$ represents an L_2 norm, and α is a parameter used to adjust the iteration step size.

Step 3. The Gram–Schmidt orthogonalization is performed on these updated initial perturbations, and $u_{0_i}^{(k)}\perp u_{0_j}^{(k)}, i\neq j$; the constraint condition in Eq. (5) is used to scale the updated initial perturbations.

Repeating steps 2 and 3, final O-CNOPs can be obtained until little change occurs in the values of the objec-

tive functions (or the gradient $\nabla J \approx 0$) with an increasing number of iterative steps. To assist the reader, in Fig. 1, we provide a schematic for computing the O-CNOPs by using the parallel iterative method.

From the above steps, although the Gram–Schmidt orthogonalization is introduced to realize the output of mutually orthogonal initial perturbations, the O-CNOPs generated by the parallel iterative method (hereafter, Para-CNOPs) are not necessarily the same as those produced by the sequential optimization method of a traditional optimization solver such as SPG2 (hereafter, SPG2-CNOPs). In ensemble forecasts, a growing-type initial perturbation is generally superimposed on the control forecast to offset its initial analysis error to achieve an ensemble forecasting member approaching the truth run. However, one cannot obtain a growing-type initial perturbation that can exactly capture the growth behavior of the initial analysis error. In this circumstance, one has to calculate the achievable initial perturbations for optimal growth, such as SPG2-CNOPs. SPG2-CNOPs have been shown to result in much higher ensemble forecasting skills than those produced by the traditional SVs and BVs methods in typhoon and ENSO forecasts (see Introduction). We subsequently ask whether Para-CNOPs can achieve similar or even higher ensemble forecasting skills than those of SPG2-CNOPs. Next, we demonstrate the advantages of Para-CNOPs from two perspectives: comparisons of the ensemble forecasting skills generated by Para-CNOPs and SPG2-CNOPs and of the timeliness of Para-CNOPs and SPG2-CNOPs for ensemble forecasts.

3. Advantages of the Para-CNOPs

In this section, we examine the Para-CNOPs by using the conceptual model presented in Lorenz (1996). The Lorenz-96 model describes the main characteristics of atmospheric motions and has been widely applied in theoretical studies on predictability associated with error growth dynamics (Boffetta et al., 1998; Lorenz and Emanuel, 1998; Vannit-

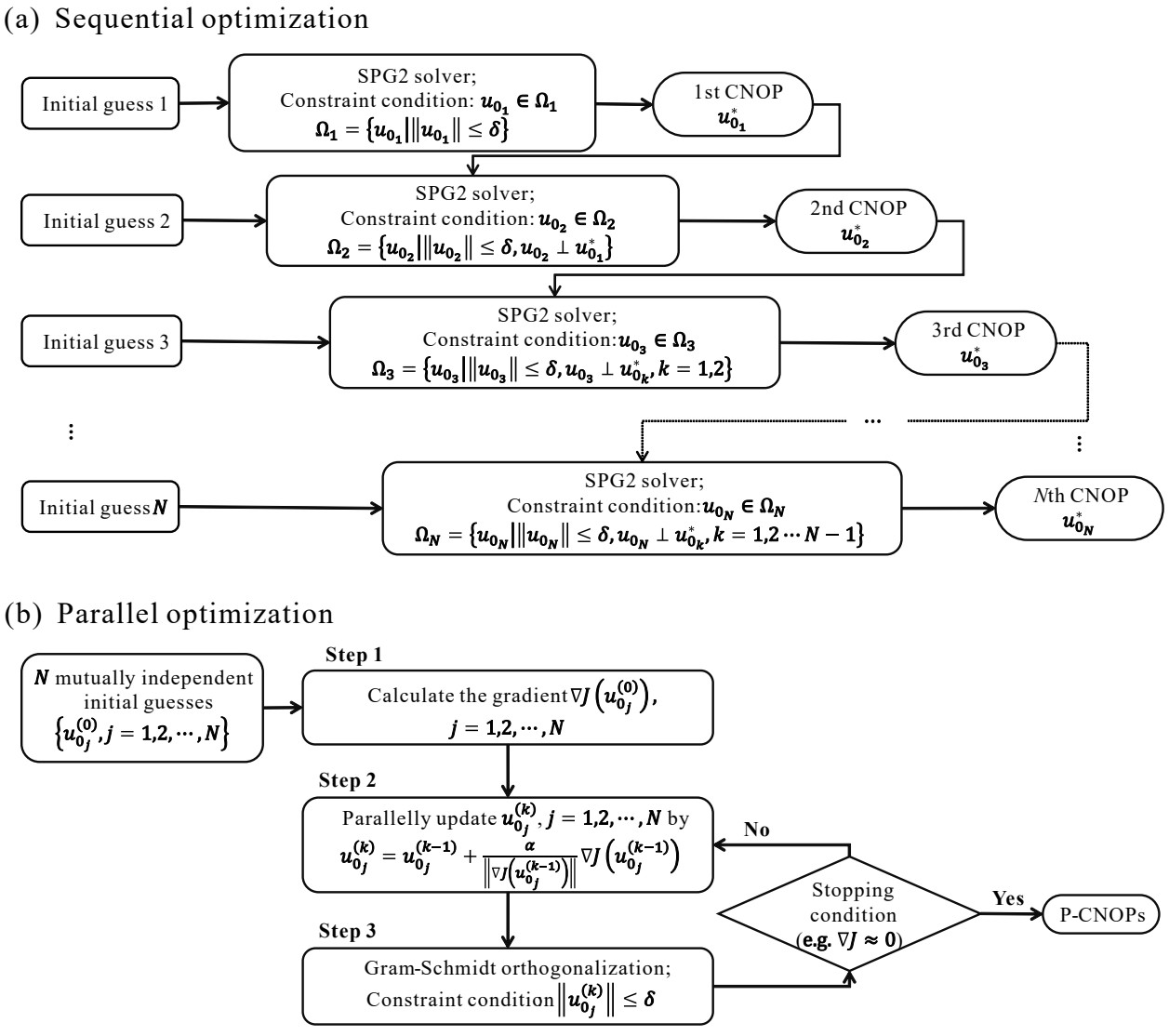

Fig. 1. Diagrams for calculating (a) SPG2-CNOPs and (b) Para-CNOPs.

sem and Toth, 2002; Orrell, 2003), and data assimilation (Anderson, 2001; Whitaker and Hamill, 2002; Hunt et al., 2004; Fertig et al., 2007). This model has also been used to explore the usefulness of new methods for ensemble forecasts (Descamps and Talagrand, 2007; Revelli et al., 2010; Basnarkov and Kocarev, 2012; Feng et al., 2014; Duan and Huo, 2016; Grudzien et al., 2020; Duan et al., 2022). In this paper, we follow these researchers and also adopt the Lorenz-96 model.

The Lorenz-96 model equation is as follows:

$$\frac{\mathrm{d}X_l}{\mathrm{d}t} = (X_{l+1} - X_{l-2})X_{l-1} - X_l + F\,, \tag{8}$$

where $l = 1, 2, \cdots, L$ ($L \in \mathbb{N}$ is the dimension of the state space), and the variable X_l satisfies cyclic boundary conditions, i.e., $X_{-1} = X_{L-1}, X_0 = X_L$, and $X_1 = X_{L+1}$, which can be thought of as representing nondimensional meteorological quantities (e.g., temperature, pressure, vorticity, and gravitational potential) that are equally spaced along a latitudinal circle. The linear term and constant term F describe the internal dissipation of the atmosphere and the external forcing, respectively.

Throughout the present study, the dimension and forcing term are chosen as $L = 40$ and $F = 8$, respectively; the model is integrated by using a fourth-order Runge–Kutta scheme with a nondimensional time step of 0.05 time units (approximately 0.25 days). With this configuration, the model solution reflects a chaotic dynamic, and is commonly used to simulate atmospheric dynamics over a single latitudinal circle, such as the dynamical behavior of vorticity, temperature, and gravitational potential (Lorenz, 1996; Lorenz and Emanuel, 1998).

3.1. *Experimental strategy*

We evaluate the Para-CNOPs based on ensemble forecasts. The Lorenz-96 model is assumed to be perfect for producing the "truth runs" to be predicted. After a spin-up run of 14 600 time steps (i.e., 10 model years), the Lorenz-96 model is further integrated for 292 000 time steps, resulting in a 200-year time series of the state variable $X_l (l = 1, 2, \cdots, L)$. Subsequently, we select the state values of $X_l (l = 1, 2, \cdots, L)$ at every 1460 time steps (i.e., one model year) as the initial values, then integrate the model forward at 40 time steps (i.e., 10 days). This process yields 200 "truth runs".

We generate the initial values of the forecasts by assimilating observations. For the Lorenz-96 model, the corresponding "observations" must be synthetic. Specifically, the "observations" here are generated by introducing random noise (as observational errors), which is sampled from a standard normal distribution $N(0, 1)$, on each of the 40 variables for the truth runs at each time step. Then, the four-dimensional variational data assimilation (4D-Var) technique is applied to the Lorenz-96 model to assimilate the "observations" and to generate the initial analysis fields for the forecasts. By using these initial analysis fields, the Lorenz-96 model is integrated for a period of 10 days, producing the control forecasts for the 200 truth runs. Due to the presence of observational errors, initial analysis errors are inevitable in control forecasts.

O-CNOPs are generally superimposed on control forecasts to execute ensemble forecasts [see Duan and Huo (2016)]. The O-CNOPs of the control forecasts are calculated in terms of their constraint radius (i.e., the positive constant numbers δ) and optimization time periods [0, T] [see Eqs. (4) and (5)]. According to Wang and Duan (2019), when $\delta = 0.8\delta_a$ (δ_a represents the amplitude of the initial analysis error measured by the L_2 norm), $T = 4$, and $N = 21$ (i.e., the number of O-CNOPs), the highest ensemble forecasting skills are statistically obtained. In this study, we adopt this configuration to compute the O-CNOPs, which, together with their negative patterns, are superimposed on the initial analysis fields to produce 42 perturbed forecasts for each control forecast. These perturbed forecasts, combined with the control forecast itself, form a group of 43 members of ensemble forecasts.

Several metrics are adopted to evaluate the quality of the ensemble forecasts. Specifically, the root-mean-square error (RMSE) and the anomaly correlation coefficient (ACC) are used to estimate the deterministic forecast skill; the Brier score (BS; Brier, 1950) and the relative operating characteristic curve area (ROCA; Mason, 1982) are adopted to measure the probabilistic forecast skill. The RMSE and BS are negatively oriented (i.e., the smaller the value, the higher the ensemble forecast skill), while the ACC and ROCA are positively oriented (i.e., the larger the value, the higher the ensemble forecast skill). The details of these four skill measurements can be found in Appendix A [also see Duan and Huo (2016) and Duan et al. (2022)].

3.2. *Comparison of the ensemble forecasting skills of Para-CNOPs and SPG2-CNOPs*

With the strategy from the last section, we conducted ensemble forecasting experiments involving 200 truth runs for a duration of 10 days to evaluate the effectiveness of the Para-CNOPs, where the hyperparameter α is experimentally set to 0.05 and the maximum iteration number is limited to 300 [see section 2, Eq. (7)]. Then, we compared the forecasting skills achieved by the Para-CNOPs and SPG2-CNOPs. Figure 2 plots the time-dependent RMSE and ACC for ensemble mean forecasts, and BS and ROCA for probabilistic forecast skills, which are averaged for the 200 truth runs when the constraint radius is $0.8\delta_a$ (see section 3.1). The results demonstrate that the ensemble forecasting skills achieved by Para-CNOPs are almost identical to those achieved by SPG2-CNOPs. This result implies that Para-CNOPs can achieve forecast capabilities comparable to those of SPG2-CNOPs at each forecasting time.

To further demonstrate the usefulness of the Para-CNOPs approach, we calculate the RMSE, ACC, BS, and ROCA values averaged across all the truth runs and lead times ranging from 0 to 10 days (see Fig. 3), where the constraint radius of $0.8\delta_a$ is used (see section 3.1); and besides

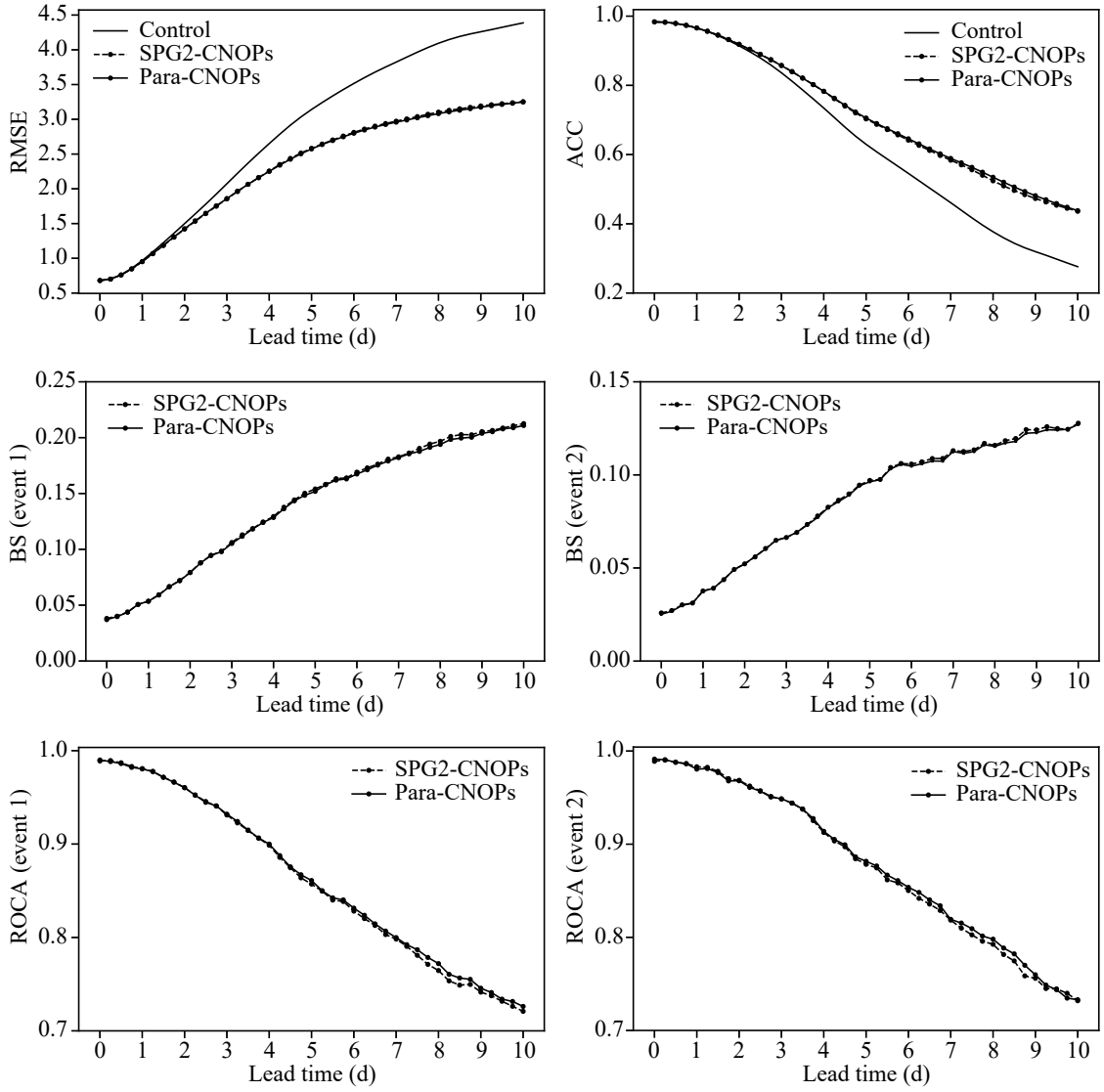

Fig. 2. The time-dependent RMSE, ACC, BS and ROCA of the ensemble forecasts generated by SPG2-CNOPs (dashed line) and Para-CNOPs (solid line) averaged over 200 truth runs. The amplitude of the CNOPs is $0.8\delta_a$. The black lines are the control forecasts.

this, the constraint radii of $0.6\delta_a$ and $1.0\delta_a$ are also adopted. The results show that the ensemble forecasts generated by the Para-CNOPs possess slightly smaller RMSE and BS values, and slightly greater ACC and ROCA values than those produced by the SPG2-CNOPs. This means that the Para-CNOPs achieve slightly higher scores compared with the SPG2-CNOPs. It is known that growing-type initial perturbations are necessary in ensemble forecasts to estimate the growth of analysis errors. However, it is impossible to obtain initial perturbations that exactly capture the growth behavior of analysis errors. Therefore, optimally growing initial perturbations, such as CNOPs, have to be calculated. Although Para-CNOPs are not always the SPG2-CNOPs, they have the possibility to depict the growth behavior of the analysis errors very well. This may explain why the Para-CNOPs achieve slightly higher scores. In any case, the scores obtained by the Para-CNOPs and SPG2-CNOPs are of trivial difference despite the former being slightly larger, suggesting that the Para-CNOPs have an almost equivalent forecasting ability to the SPG2-CNOPs.

In addition to the ensemble forecast skill measured by the above skill measurements, the reliability of the ensemble members is also a key aspect that reflects the advantages of a new ensemble forecasting method. We therefore proceed to explore the reliability of the ensemble members generated by the Para-CNOPs. In previous studies, researchers have shown that reliable ensemble members should exhibit an ensemble spread that is nearly equal to the RMSE of the ensemble mean (see Appendix B; Bowler, 2006; Leutbecher and Palmer, 2008; Fortin et al., 2014; Hopson, 2014). To address this issue for Para-CNOPs, the ratios of the ensemble spread to the RMSE for Para-CNOPs and SPG2-CNOPs are presented in Fig. 4 for the constraint radius of $0.8\delta_a$. Let us note that Fig. 4a plots the temporal variability of the ratio

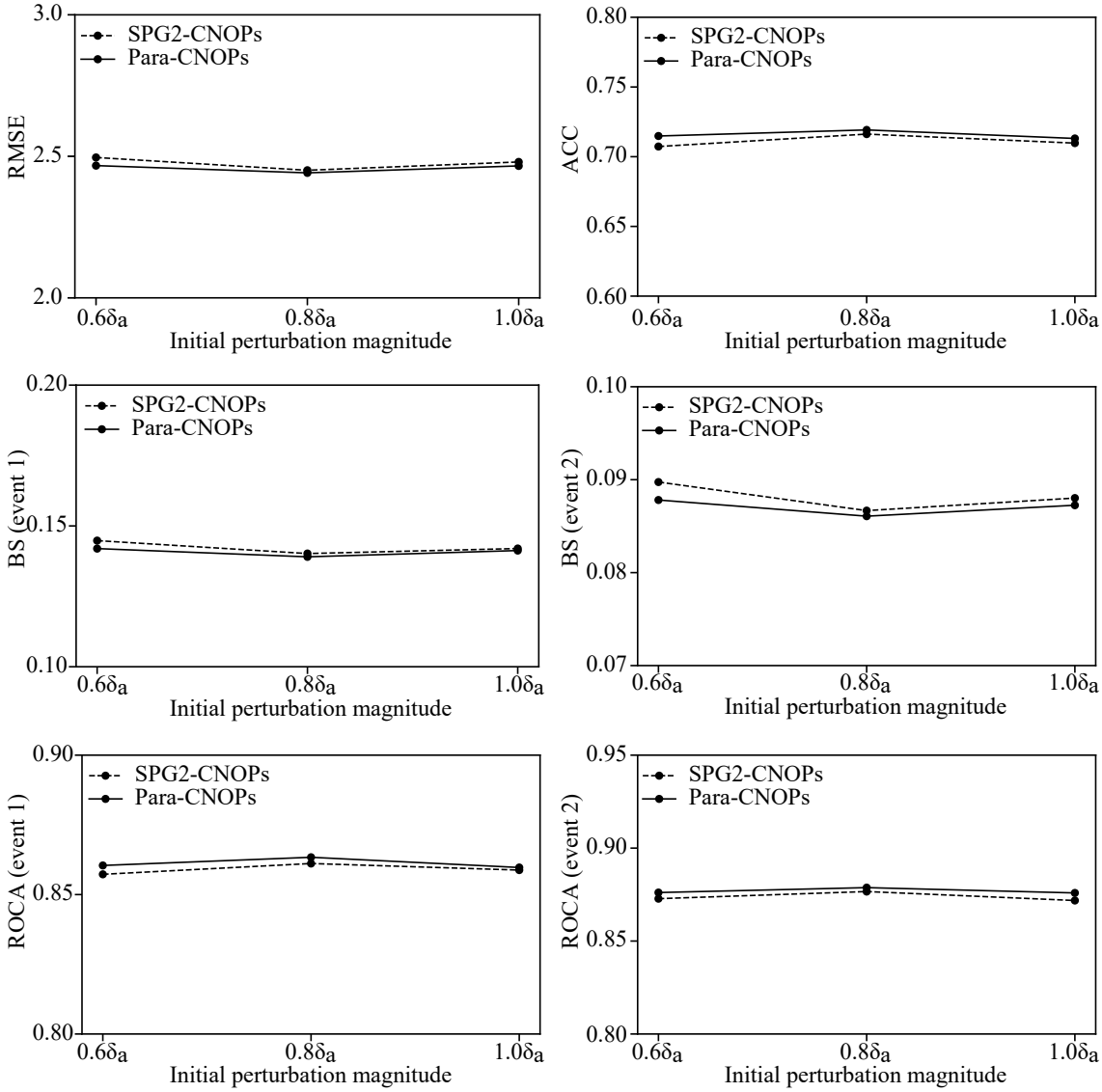

Fig. 3. Performances of the ensemble forecasts generated by SPG2-CNOPs (dashed line) and Para-CNOPs (solid line) averaged over 200 truth runs and all lead times. The horizontal axis denotes the constraint radius, and the vertical axis represents the RMSE, ACC, BS and ROCA values.

averaged for all truth runs, while Fig. 4b gives the spatial variability of the ratio averaged for all truth runs and lead times. The ratios for both Para-CNOPs and SPG2-CNOPs are almost identical and close to 1. This suggests that Para-CNOPs provide ensemble members with reliability similar to that of SPG2-CNOPs and indicates that Para-CNOPs can offer a reasonable estimation of forecast uncertainties in both time and space by using their ensemble spread.

We have to acknowledge that neither the SPG2-CNOPs and Para-CNOPs provide a flatter ratio of the ensemble spread to the RMSE at the initial stage of forecasts (see Fig. 4a). As discussed above, growing-type initial perturbations are necessary in ensemble forecasts and achievable optimally growing initial perturbations have to be calculated. In Fig. 4, both SPG2-CNOPs and Para-CNOPs are calculated with $\delta = 0.8\delta_a$, along with $T = 4$, and $N = 21$, to make the ensemble forecasts generated by the CNOPs achieve the highest skill averaged over the whole forecast periods for all truth runs (see section 3.1). However, the initial perturbation amplitude, $\delta = 0.8\delta_a$, tends to underestimate the initial analysis error amplitude, δ_a, and then results in the ratio of the ensemble spread to the RMSE being less than 1 at the initial time of forecasts. Despite these smaller CNOPs, they represent the optimally growing initial perturbations; in particular, from Fig. 4a it is clear that the ratio of the ensemble spread to the RMSE is larger than 1 at the optimization time $T = 4$. This indicates that the smaller CNOPs have much larger growth than the initial analysis errors at $T = 4$, and cause an overestimation of the analysis error at $T = 4$. All these factors may explain the transition of the ratio from being less than 1 to being larger than 1 at the initial stage of the forecasts, as shown in Fig. 4a. Nonetheless, the ratio still remains within an acceptable range of [0.8, 1.2], indicating the reliability of the ensemble members.

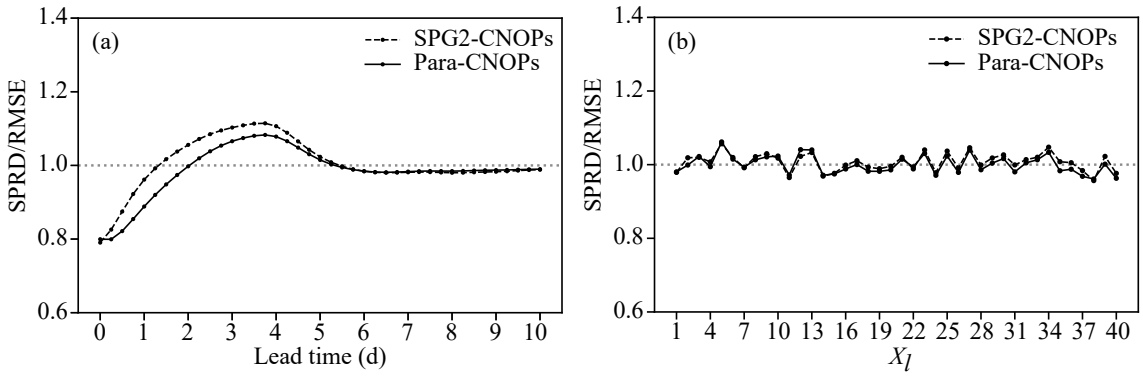

Fig. 4. The (a) temporal and (b) spatial variabilities in the ratio of the ensemble spread to the RMSE obtained by SPG2-CNOPs (dashed line) and Para-CNOPs (solid line), where the variabilities are calculated by averaging over the 200 truth runs; in particular, the spatial variabilities are obtained through further averaging over the lead times ranging from 0 to 10 days.

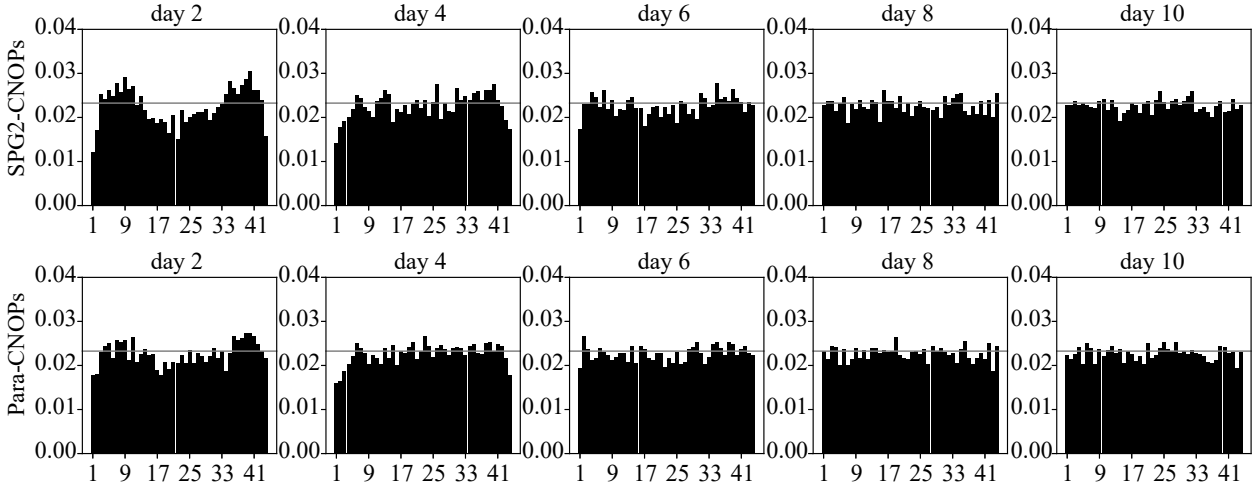

Fig. 5. Talagrand diagrams for the ensemble forecasts made by SPG2-CNOPs (top row) and Para-CNOPs (bottom row) at lead times of 2, 4, 6, 8 and 10 days.

Another measure of the reliability of ensemble members is the Talagrand diagram (see Appendix B; Talagrand et al., 1997; Candille and Talagrand, 2005). The flatter the relevant histogram, the more reliable the ensemble members. Figure 5 shows the Talagrand diagrams for Para-CNOPs and SPG2-CNOPs at various lead times. The Para-CNOPs exhibit a flat histogram almost identical to that of the SPG2-CNOPs. This indicates that the Para-CNOPs provide ensemble members as reliably as do the SPG2-CNOPs for ensemble forecasts.

3.3. *Comparison of the timeliness of computing Para-CNOPs and SPG2-CNOPs*

The timely computation of optimal initial perturbations is frequently challenging in ensemble forecast scenarios. Therefore, developing a highly effective and efficient method for solving the optimal initial perturbations for ensemble forecasts is urgently important. In this section, we compare the time consumed for obtaining Para-CNOPs and SPG2-CNOPs to validate the efficiency of Para-CNOPs. In Fig. 6, we provide box-and-whisker plots for their respective computation times, where the data represent the computational times of 21 CNOPs for one truth run and are obtained by averaging over the 200 truth runs. The calculations are based on Fortran Code and Intel(R) Xeon(R) CPU E7-4870 v2 @2.30 GHz. The results show that calculating SPG2-CNOPs generally requires approximately 279.18 s.

For the Para-CNOPs, since the calculation allows the use of multiple computer cores to obtain O-CNOPs via a parallel method, we first examine the time consumed for calculating the Para-CNOPs by using varying numbers of computer cores in parallel (see Fig. 7). The results show that parallel computing can indeed effectively decrease the time consumed for calculations. Nevertheless, we find that the time consumed does not decay linearly with the increasing number of computer cores. In fact, it is at 24 computer cores that the decay of the time consumed for computing the Para-CNOPs reaches saturation. This indicates that the addition of fewer computer cores can help parallel iterative methods significantly increase the computational efficiency of Para-CNOPs, even under practical circumstances. Specifically, we adopt 24 computer cores for approximately 2.05 s for com-

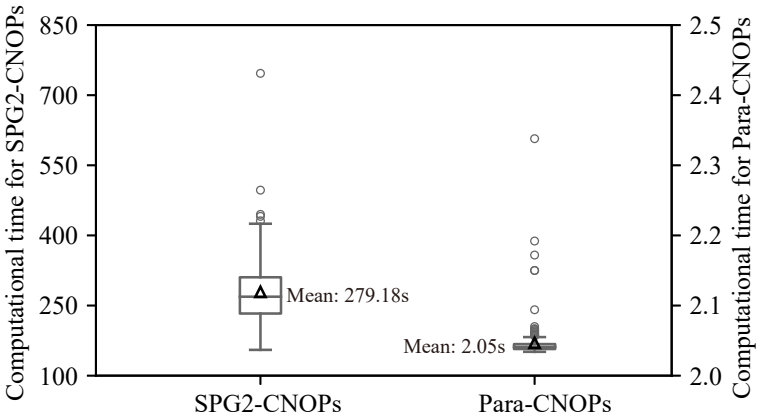

Fig. 6. Comparison of the computation times of the SPG2-CNOPs and Para-CNOPs. One computing core is used for SPG2-CNOPs, and 24 computing cores are used for Para-CNOPs. The box-and-whisker plot illustrates the distribution of the time consumed for computing the O-CNOPs of 200 truth runs. Each data point in the figure represents the time needed to compute 21 O-CNOPs for one truth run. The box extends from the first quartile to the third quartile, with the solid line in the box indicating the median and a triangle marking the mean. The whiskers represent the range, reaching to the farthest data point lying within 1.5 times the interquartile range from the box, and further small circles beyond the whiskers are considered outliers. The left and right vertical axes represent the times consumed for computing SPG2-CNOPs and Para-CNOPs, respectively.

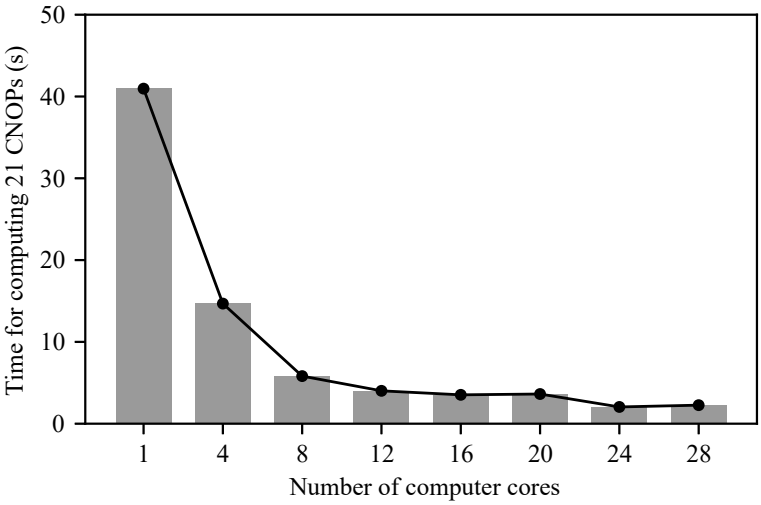

Fig. 7. The time taken to compute 21 Para-CNOPs of one truth run as a function of the number of computer cores, obtained by averaging the 200 truth runs.

puting 21 CNOPs in one truth run (see Fig. 6). It is obvious that the Para-CNOPs calculations greatly reduce the time consumed by the SPG2-CNOPs and can be aggressively calculated with high efficiency. Furthermore, from section 3.2, it is known that the Para-CNOPs can achieve an ensemble forecast ability as high as that of the SPG2-CNOPs. Therefore, Para-CNOPs provide a method that can highly efficiently yield growing-type initial perturbations for ensemble forecasting; and moreover, they achieve high ensemble forecasting skill.

4. Discussion

The above results show that Para-CNOPs can provide reliable ensemble members and can achieve ensemble forecasting skills as high as those of SPG2-CNOPs. In fact, in numerical experiments, we also explore the magnitudes of the nonlinear evolution of Para-CNOPs, i.e., the value of the cost function $J(u_0)$, and we compare them with those of SPG2-CNOPs. We find that the Para-CNOPs possess similar dynamical growth as SPG2-CNOPs. Specifically, in Fig. 8, we plot the values of the cost function $J(u_0)$ with respect to

the Para-CNOPs. Then, we find that they have $J\left(u_{0_1}^*\right) > J\left(u_{0_2}^*\right) > \cdots > J\left(u_{0_n}^*\right)$ values, which are very similar to those of SPG2-CNOPs; furthermore, their values are not far from those of SPG2-CNOPs, especially for the latter-order CNOPs. However, when we directly compare the Para-CNOPs with the SPG2-CNOPs for each truth run, we find that they are not always of similar patterns due to their solvers having different optimization capacities. The tool of perturbation versus error correlation analysis (PECA; see Appendix C) is further applied to examine the ability of the Para-CNOPs in interpreting the analysis errors, and the results show that the PECA of Para-CNOPs matches that of SPG2-CNOPs to a large extent (see Fig. 9). This indicates that, despite the Para-CNOPs not always being the SPG2-CNOPs, the ensemble generated by them can also approximately describe the analysis error. In this situation, we regard the Para-CNOPs as an approximation of the SPG2-CNOPs. This may explain why Para-CNOPs produce reliable ensemble members similar to SPG2-CNOPs and can achieve high ensemble forecast skill comparable to that of SPG2-CNOPs.

It is apparent that both SPG2-CNOPs and Para-CNOPs adopt $\delta = 0.8\delta_a$ to constrain their amplitudes with the initial analysis error amplitude δ_a as a reference. It should be noted that the initial amplitude of the analysis error in real-time forecasting is typically unknown. It is therefore challenging to determine appropriate initial perturbation amplitudes for ensemble forecasts. A prevalent approach is to use observations or reanalysis data as approximations of the true state and compare these with the analysis field to provide a rough estimation of initial analysis errors. This estimation is based on statistics obtained from long-term hindcast experiments, and the variance of the estimated analysis error is commonly used as a reference for the generation and tuning of initial perturbations in operational ensemble forecasts (Toth and Kalney, 1997; Leutbecher and Palmer, 2008; Yamaguchi

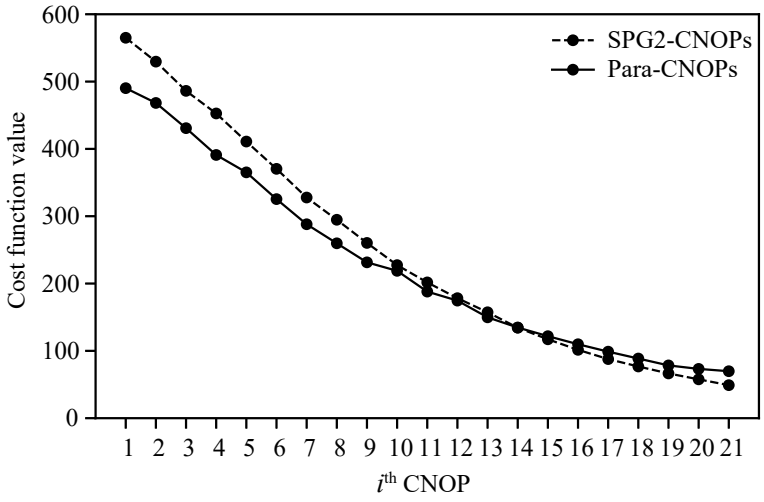

Fig. 8. Values of the cost function for SPG2-CNOPs (dashed line) and Para-CNOPs (solid line), which are averaged for 200 truth runs.

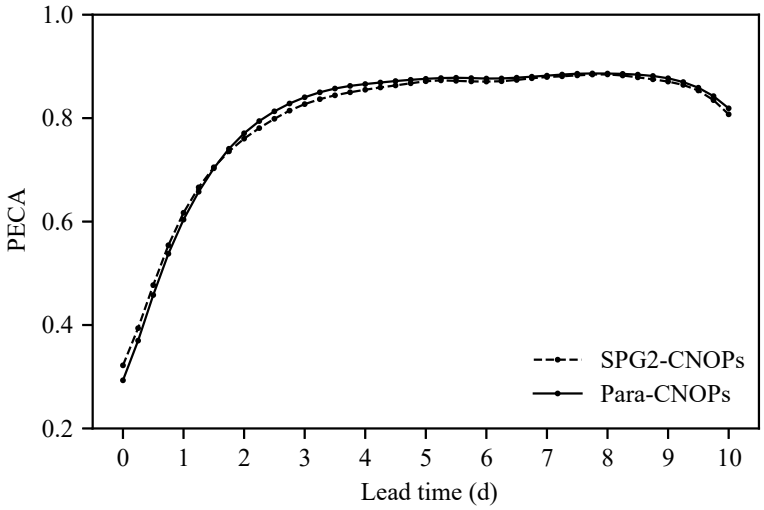

Fig. 9. The PECA values generated by SPG2-CNOPs and Para-CNOPs, which are averaged for 200 truth runs.

and Majumdar, 2010). However, the characteristics of analysis errors are not static; they vary with the flow-dependent weather regimes. Therefore, the generation of initial ensemble perturbations should also consider such variation and constraints. Ensemble data assimilation methods, such as the ensemble Kalman filter (EnKF), can provide an estimate of flow-dependent analysis errors using the spread of a posterior ensembles. Nonetheless, these a posterior ensembles heavily rely on various empirical parameters set within the EnKF system and may provide biased error estimation due to the limited number of ensemble members (Li et al., 2009; Peña and Toth, 2014; Hoteit et al., 2015; Feng et al., 2017). Recently, Feng et al. (2023) proposed the use of a Statistical Analysis and Forecast Error method for quantifying analysis errors of operational forecast systems. This process may provide effective estimates of the flow-dependent analysis errors, and then facilitate the recognition of more reasonable initial perturbation amplitudes for ensemble forecasts. In any case, accurately estimating analysis errors, particularly those that are flow-dependent, remains a significant challenge for refining the generation of initial ensemble perturbations.

5. Summary

In this study, we propose a new iterative method for computing O-CNOPs in an attempt to greatly reduce the computational time. This method incorporates a gradient-based iteration approach with Gram–Schmidt orthogonalization, and allows the use of a parallel algorithm to significantly increase the timeliness of implementing O-CNOPs in ensemble forecasts. In fact, when we compare the computation time of computing O-CNOPs by using the original sequential optimization method and the parallel optimization method in the present study, the latter is found to be a very small part of the former. Specifically, when we compute the 21 O-CNOPs for one truth run requested by the ensemble forecasts generated by the Lorenz-96 model, the sequential method takes approximately 279 s using one computing core, while the parallel method takes only approximately 2 s to run with 24 computing cores. Therefore, the parallel iterative optimization method proposed in this study is highly efficient and can greatly increase the timeliness of implementing O-CNOPs in real ensemble forecasts.

In comparison to sequentially optimized O-CNOPs (SPG2-CNOPs), parallelly optimized O-CNOPs (Para-CNOPs) have been shown to provide reliable ensemble members with an ensemble forecasting ability comparable to that of SPG2-CNOPs. This highlights the effectiveness of the proposed approach in obtaining ensemble forecasting skills as high as those of SPG2-CNOPs. For this purpose, we investigate the evolution of Para- and SPG2-CNOPs. We find that they exhibit highly similar dynamic growths. That is, the amplitudes of Para-CNOPs growths are very close to those of SPG2-CNOPs; furthermore, they are ranked with the same sequence as SPG2-CNOPs. Particularly, the Para-CNOPs are demonstrated to provide an ensemble that is similar to that generated by the SPG2-CNOPs and can appropriately address analysis errors. These findings may explain why the Para-CNOPs can produce reliable ensemble members, as can the SPG2-CNOPs, and why the Para-CNOPs achieve high ensemble forecast skill comparable to that of the SPG2-CNOPs.

The high efficiency and effectiveness of implementing Para-CNOPs may support their applicability in realistic ensemble forecasts. Therefore, in subsequent studies, we plan to extend the Para-CNOPs to more realistic weather and climate models to investigate the applicability of Para-CNOPs in ensemble forecasts, especially for high-impact weather and climate events. It is conceivable from section 3.3 that we can compute the Para-CNOPs using a very small part of the computation time for calculating SPG2-CNOPs. Zhang et al. (2023a) showed that, for the Weather Research and Forecasting (WRF) model with a horizontal grid spacing of 60 km and a coarser vertical resolution of 15 vertical levels with the top level at 50 hPa, the calculation of 21 CNOPs with 64 computing cores for one five-day forecast takes nearly 2 h when the CNOPs are calculated one by one. From the comparison between Para-CNOPs and SPG2-CNOPs in section 3.3, it is indicated that the calculation of the 21 Para-CNOPs with enough computing cores for one forecast in the WRF model needs at most the time of calculating one of the SPG2-CNOPs using 64 computing cores [i.e. about 6 min; also see Zhang et al. (2023a)]. Therefore, it is expected that Para-CNOPs can be applied in realistic complex models for efficiently conducting ensemble forecasts.

In addition, the O-CNOPs address the effect of initial uncertainties. In practical forecasts, model errors that limit the ensemble forecasting ability are also important factors. Furthermore, model errors interact with initial errors to further amplify forecast uncertainties. Duan et al. (2022) proposed an approach with nonlinear forcing singular vectors that combines initial and model perturbations (C-NFSVs) to reveal the combined effect of initial and model errors. C-NFSVs can be divided into two special cases: O-CNOPs, which consider only initial error effects (Duan and Huo, 2016); and orthogonal NFSVs, which involve only model error effects (O-NFSVs; Zhang et al., 2023b). Since the C-NFSV and its special case of O-NFSV are both relevant to model errors at each time step of numerical integration, their optimizations are much more time-consuming for ensemble forecasts. However, it is gratifying that the above parallel iterative optimization method can be easily extended to calculate C-NFSVs and O-NFSVs to greatly increase the timeliness of implementing them in ensemble forecasts. Therefore, we expect that these optimal perturbation methods can be effectively implemented in realistic ensemble forecasts with the help of the parallel iterative optimization method.

Acknowledgements. The authors thank the three anonymous reviewers very much for their insightful comments and suggestions. This work was sponsored by the National Natural Science Foundation of China (Grant Nos. 41930971, 42330111, and 42405061) and the National Key Scientific and Technological Infrastructure project "Earth System Numerical Simulation Facility"

(EarthLab).

APPENDIX A

A1. Root-mean-square error of the ensemble mean

The ensemble mean is calculated as follows. Let $\overline{X}_l$ be the ensemble mean of the lth component of the N members:

$$\overline{X}_l = \frac{1}{N}\sum_{n=1}^{N} X_l^{(n)}, \tag{A1}$$

where $X_l^{(n)}$ represents the lth component of the nth ensemble member and $l = 1,2,\cdots,L$ and $n = 1,2,\cdots,N$. The root-mean-square error (RMSE) of the ensemble mean measures the difference between the ensemble mean $\overline{X}_l$ and the observations O_l (i.e., the truth runs in the present study) and is defined as follows:

$$\mathrm{RMSE} = \sqrt{\frac{1}{R}\sum_{r=1}^{R}\frac{1}{L}\sum_{l=1}^{L}\left(\overline{X}_{l,r} - O_{l,r}\right)}, \tag{A2}$$

where R represents the number of realizations.

A2. Anomaly correlation coefficient

The anomaly correlation coefficient (ACC) is used to measure the similarity between the forecasted and the observed anomalies. The ACC is calculated as follows:

$$\mathrm{ACC} = \frac{\sum_{l=1}^{L}\left(X_l' - \overline{X'}\right)\left(O_l' - \overline{O'}\right)}{\sqrt{\sum_{l=1}^{L}\left(X_l' - \overline{X'}\right)^2\left(O_l' - \overline{O'}\right)^2}}, \tag{A3}$$

where $X_l' = X_l - C_l^X$ and $O_l' = O_l - C_l^O$. X_l is the forecast value; O_l is the observation; C_l^X is the model climatological state; C_l^O is the observed climatological state; X_l' is the forecasted anomaly; and O_l' is the observed anomaly. The larger the ACC, the higher the forecast skill.

A3. Brier score

The Brier score (BS) is the mean-square error of the probability forecast and is defined as follows:

$$\mathrm{BS} = \frac{1}{R}\sum_{r=1}^{R}(f_r - o_r)^2, \tag{A4}$$

where R is the number of realizations of the prediction process and f_r and o_r are the probability of the forecast and the observation, respectively, for the rth prediction process. A smaller BS indicates a better probability forecast skill.

A4. Relative operating characteristic curve area

The relative operating characteristic curve area (ROCA) is a measure of the resolution of a prediction system. By considering whether an event occurs at every grid point and checking the forecasts against the observations, we can construct a two-category contingency table (see Table A1), where a and b represent the number of hits and false alarms, respectively, and c and d represent the number of misses and correct rejections, respectively.

Table A1. Two-by-two contingency table of a binary event.

	Observation		
Forecast	Yes	No	Total
Yes	a	b	$a+b$
No	c	d	$c+d$
Total	$a+c$	$b+d$	

Then, the hit rate and the false alarm rate can be calculated as in Eq. (A5) and (A6), respectively:

$$\text{Hit rate}: H = \frac{a}{(a+c)}, \tag{A5}$$

$$\text{False alarm rate}: F = \frac{b}{(b+d)}. \tag{A6}$$

The ROC curve can be obtained by the pairs H and F, and the area under the ROC curve is called the ROCA, which decreases from 1 to 0 as more false alarm occur. The ROCA is calculated as in Eq. (A7):

$$\mathrm{ROCA} = \int_0^1 H(x)\,\mathrm{d}x = \sum_{k=1}^{K}\frac{1}{2}(H_{k+1} + H_k)(F_{k+1} - F_k), \tag{A7}$$

where K is the number of categories relative to the probability thresholds. A larger ROCA value indicates a better probability forecast. When the ROCA is greater than 0.5, the forecast can be regarded as skillful.

APPENDIX B

B1. Ensemble spread and the ratio of spread to RMSE

According to subsection A1 in Appendix A, the ensemble spread is defined as follows:

$$\mathrm{SPRD} = \sqrt{\frac{1}{R}\sum_{r=1}^{R}\frac{1}{L}\sum_{l=1}^{L}\frac{1}{N-1}\sum_{n=1}^{N}\left(X_{l,r}^{(n)} - O_{l,r}\right)}, \tag{B1}$$

where the representation of the characters is consistent with Eq. (A1). The ratio of the ensemble spread to the RMSE can be defined as follows:

$$\mathrm{Ratio} = \frac{\mathrm{SPRD}}{\mathrm{RMSE}}. \tag{B2}$$

For a reliable ensemble, the ratio between the spread of the ensemble members and the RMSE of the ensemble mean approaches 1.

B2. Talagrand diagram

In the case of ensemble forecasting with N ensemble members and L grid points, these N members are ranked in ascending order, and $N + 1$ intervals can be divided on each

grid point. Observations (i.e., the truth runs in this study) on corresponding grid points will inevitably fall into a certain interval, and the numbers of observations that fall into the kth interval can be accumulated and denoted as $S_k(k = 1, 2, \cdots, N+1)$. For N ensemble members and L grid points, the valid samples can be defined as $S = NL$. Then, the probability of observations falling in the kth interval is

$$P_k = \frac{S_k}{S} . \tag{B3}$$

According to the distribution of probability P_k, the Talagrand diagram can be drawn. Theoretically, observations should fall with equal probability into each of the intervals for a perfect ensemble forecast system. Therefore, a flatter Talagrand diagram signifies a higher reliability of the ensemble forecasting system. Additionally, when the Talagrand diagram appears concave, the ensemble spread is small. Conversely, a convex shape suggests excessive spread. An obvious asymmetry in the Talagrand diagram implies bias in the ensemble.

APPENDIX C

C1. Perturbation versus error correlation analysis

Perturbation versus error correlation analysis (PECA) is commonly used to evaluate the initial perturbations by measuring their ability to explain forecast error variance, which is an appropriate tool for the comparison of ensembles generated by different schemes (Wei and Toth, 2003; Buizza et al., 2005). Ensemble perturbation is defined as the difference between perturbed forecasts and their corresponding control forecasts, which can be expressed by Eq. (C1):

$$P_i(t) = F_i(t) - F_{\text{ctrl}}(t) , \tag{C1}$$

where $P_i(t)$, $F_i(t)$, $F_{\text{ctrl}}(t)$ represent the ith ensemble perturbation, the ith ensemble forecast member, and the control forecast, respectively. The forecast errors $E(t)$ are defined as the difference between the control forecast $F_{\text{ctrl}}(t)$ and the verifying analysis $F(t)$:

$$E(t) = F_{\text{ctrl}}(t) - F(t) . \tag{C2}$$

The a posteriori optimal combination of N perturbations is obtained by solving the least-squares problem:

$$\min \left\| E - \sum_{i=1}^{N} \alpha_i P_i \right\|_2^2 . \tag{C3}$$

To solve this optimization problem, we obtain the optimal estimate values of α_i denoted as $\widehat{\alpha}_i$, along with the combination vector P_{opt} under the optimal estimation:

$$P_{\text{opt}} = \sum_{i=1}^{N} \widehat{\alpha}_i P_i . \tag{C4}$$

Then, the PECA can be calculated:

$$\text{PECA} = \frac{\text{cov}(P_i, E)}{\text{cov}(P_{\text{opt}}, P_{\text{opt}})^{1/2} \text{cov}(E, E)^{1/2}} , \tag{C5}$$

where $cov(\cdot)$ is the covariance. The larger the PECA value, the greater the ability of the ensemble perturbations to explain the forecast error variances.

REFERENCES

Anderson, J. L., 1997: The impact of dynamical constraints on the selection of initial conditions for ensemble predictions: Low-order perfect model results. *Mon. Wea. Rev.*, **125**, 2969–2983, https://doi.org/10.1175/1520-0493(1997)125<2969:Tiodco>2.0.Co;2.

Anderson, J. L., 2001: An ensemble adjustment Kalman filter for data assimilation. *Mon. Wea. Rev.*, **129**, 2884–2903, https://doi.org/10.1175/1520-0493(2001)129<2884:AEAKFF>2.0.CO;2.

Barkmeijer, J., 1996: Constructing fast-growing perturbations for the nonlinear regime. *J. Atmos. Sci.*, **53**, 2838–2851, https://doi.org/10.1175/1520-0469(1996)053<2838:Cfgpft>2.0.Co;2.

Basnarkov, L., and L. Kocarev, 2012: Forecast improvement in Lorenz 96 system. *Nonlinear Processes in Geophysics*, **19**, 569–575, https://doi.org/10.5194/npg-19-569-2012.

Birgin, E. G., J. M. Martínez, and M. Raydan, 2000: Nonmonotone spectral projected gradient methods on convex sets. *SIAM Journal on Optimization*, **10**, 1196–1211, https://doi.org/10.1137/S1052623497330963.

Boffetta, G., P. Giuliani, G. Paladin, and A. Vulpiani, 1998: An extension of the Lyapunov analysis for the predictability problem. *J. Atmos. Sci.*, **55**, 3409–3416, https://doi.org/10.1175/1520-0469(1998)055<3409:AEOTLA>2.0.CO;2.

Bowler, N. E., 2006: Comparison of error breeding, singular vectors, random perturbations and ensemble Kalman filter perturbation strategies on a simple model. *Tellus A: Dynamic Meteorology and Oceanography*, **58**(5), 538–548, https://doi.org/10.1111/j.1600-0870.2006.00197.x.

Brier, G. W., 1950: Verification of forecasts expressed in terms of probability. *Mon. Wea. Rev.*, **78**, 1–3, https://doi.org/10.1175/1520-0493(1950)078<0001:Vofeit>2.0.Co;2.

Buizza, R., and T. N. Palmer, 1995: The singular-vector structure of the atmospheric global circulation. *J. Atmos. Sci.*, **52**, 1434–1456, https://doi.org/10.1175/1520-0469(1995)052<1434:Tsvsot>2.0.Co;2.

Buizza, R., J., Tribbia, F., Molteni, and T., Palmer, 1993: Computation of optimal unstable structures for a numerical weather prediction model. *Tellus A: Dynamic Meteorology and Oceanography*, **45**(5), 388–407, https://doi.org/10.3402/tellusa.v45i5.14901.

Buizza, R., P. L. Houtekamer, G. Pellerin, Z. Toth, Y. J. Zhu, and M. Z. Wei, 2005: A comparison of the ECMWF, MSC, and NCEP global ensemble prediction systems. *Mon. Wea. Rev.*, **133**, 1076–1097, https://doi.org/ https://doi.org/10.1175/Mwr2905.1.

Candille, G., and O. Talagrand, 2005: Evaluation of probabilistic prediction systems for a scalar variable. *Quart. J. Roy. Meteor. Soc.*, **131**, 2131–2150, https://doi.org/10.1256/qj.04.71.

Chan, P. W., W. Han, B. Mak, X. H. Qin, Y. Z. Liu, R. Y. Yin, and J. C. Wang, 2023: Ground-space-sky observing system experiment during tropical cyclone Mulan in August 2022. *Adv. Atmos. Sci.*, **40**, 194–200, https://doi.org/10.1007/

s00376-022-2267-z.

Chen, G., B. Wang, and J. J. Liu, 2021: Study on the sensitivity of initial perturbations to the development of a vortex observed in Southwest China. *J. Geophys. Res.: Atmos.*, **126**, e2021JD034715, https://doi.org/10.1029/2021JD034715.

Descamps, L., and O. Talagrand, 2007: On some aspects of the definition of initial conditions for ensemble prediction. *Mon. Wea. Rev.*, **135**, 3260–3272, https://doi.org/10.1175/Mwr3452.1.

Du, J., and Coauthors, 2018: Ensemble methods for meteorological predictions. *Handbook of Hydrometeorological Ensemble Forecasting*, Q. Duan et al., Eds., Springer, 1–52, https://doi.org/10.1007/978-3-642-40457-3_13-1.

Duan, Q. Y., F. Pappenberger, A. Wood, H. L. Cloke, and J. C. Schaake, 2019: *Handbook of Hydrometeorological Ensemble Forecasting*. Springer, 1528 pp, https://doi.org/10.1007/978-3-642-39925-1.

Duan, W. S., and R. Zhang, 2010: Is model parameter error related to a significant spring predictability barrier for El Nino events? Results from a theoretical model. *Adv. Atmos. Sci.*, **27**, 1003–1013, https://doi.org/10.1007/s00376-009-9166-4.

Duan, W. S., and F. F. Zhou, 2013: Non-linear forcing singular vector of a two-dimensional quasi-geostrophic model. *Tellus A: Dynamic Meteorology and Oceanography*, **65**, 18452, https:// https://doi.org/10.3402/tellusa.v65i0.18452.

Duan, W. S., and Z. H. Huo, 2016: An approach to generating mutually independent initial perturbations for ensemble forecasts: Orthogonal conditional nonlinear optimal perturbations. *J. Atmos. Sci.*, **73**, 997–1014, https://doi.org/10.1175/Jas-D-15-0138.1.

Duan, W. S., M. Mu, and B. Wang, 2004: Conditional nonlinear optimal perturbations as the optimal precursors for El Nino-southern oscillation events. *J. Geophys. Res.: Atmos.*, **109**, D23105, https://10.1029/2004JD004756.

Duan, W. S., X. Q. Li, and B. Tian, 2018: Towards optimal observational array for dealing with challenges of El Niño-Southern Oscillation predictions due to diversities of El Niño. *Climate Dyn.*, **51**, 3351–3368, https://doi.org/10.1007/s00382-018-4082-x.

Duan, W. S., J. J. Ma, and S. Vannitsem, 2022: An ensemble forecasting method for dealing with the combined effects of the initial and model errors and a potential deep learning implementation. *Mon. Wea. Rev.*, **150**, 2959–2976, https://doi.org/10.1175/MWR-D-22-0007.1.

Duan, W. S., L. C. Yang, Z. Z. Xu, and J. Chen, 2023b: Conditional nonlinear optimal perturbation: Applications to ensemble forecasting of high-impact weather systems. *Numerical Weather Prediction: East Asian Perspectives*, S. K. Park, Ed., Springer, 441–460, https://doi.org/10.1007/978-3-031-40567-9_17.

Duan, W. S., L. C. Yang, M. Mu, B. Wang, X. S. Shen, Z. Y. Meng, and R. Q. Ding, 2023a: Recent advances in China on the predictability of weather and climate. *Adv. Atmos. Sci.*, **40**, 1521–1547, https://doi.org/10.1007/s00376-023-2334-0.

Epstein, E. S., 1969: Stochastic dynamic prediction. *Tellus A: Dynamic Meteorology and Oceanography*, **21**, 739–759, https://doi.org/10.3402/tellusa.v21i6.10143.

Feng, J., Z. Toth, and M. Peña, 2017: Spatially extended estimates of analysis and short-range forecast error variances. *Tellus A: Dynamic Meteorology and Oceanography*, **69**(1), 1325301, https://doi.org/10.1080/16000870.2017.1325301.

Feng, J., R. Q. Ding, D. Q. Liu, and J. P. Li, 2014: The application of nonlinear local Lyapunov vectors to ensemble predictions in Lorenz systems. *J. Atmos. Sci.*, **71**, 3554–3567, https://doi.org/10.1175/Jas-D-13-0270.1.

Feng, J., J. C. Wang, G. K. Dai, F. F. Zhou, and W. S. Duan, 2023: Spatiotemporal estimation of analysis errors in the operational global data assimilation system at the China Meteorological Administration using a modified SAFE method. *Quart. J. Roy. Meteor. Soc.*, **149**(755), 2301–2319, https://doi.org/10.1002/qj.4507.

Feng, J., X. H. Qin, C. Q. Wu, P. Zhang, L. Yang, X. S. Shen, W. Han, and Y. Z. Liu, 2022: Improving typhoon predictions by assimilating the retrieval of atmospheric temperature profiles from the FengYun-4A's Geostationary Interferometric Infrared Sounder (GIIRS). *Atmospheric Research*, **280**, 106391, https://doi.org/10.1016/j.atmosres.2022.106391.

Fertig, E. J., J. Harlim, and B. R. Hunt, 2007: A comparative study of 4D-VAR and a 4D ensemble Kalman filter: Perfect model simulations with Lorenz-96. *Tellus A: Dynamic Meteorology and Oceanography*, **59**(1), 96–100, https://doi.org/10.1111/j.1600-0870.2006.00205.x

Fortin, V., M. Abaza, F. Anctil, and R. Turcotte, 2014: Why should ensemble spread match the RMSE of the ensemble mean?. *Journal of Hydrometeorology*, **15**, 1708–1713, https://doi.org/10.1175/Jhm-D-14-0008.1.

Grudzien, C., M. Bocquet, and A. Carrassi, 2020: On the numerical integration of the Lorenz-96 model, with scalar additive noise, for benchmark twin experiments. *Geoscientific Model Development*, **13**, 1903–1924, https://doi.org/10.5194/gmd-13-1903-2020.

Hamill, T. M., C. Snyder, and R. E. Morss, 2000: A comparison of probabilistic forecasts from bred, singular-vector, and perturbed observation ensembles. *Mon. Wea. Rev.*, **128**, 1835–1851, https://doi.org/10.1175/1520-0493(2000)128<1835:Acopff>2.0.Co;2.

Hopson, T. M., 2014: Assessing the ensemble spread-error relationship. *Mon. Wea. Rev.*, **142**, 1125–1142, https://doi.org/10.1175/Mwr-D-12-00111.1.

Hoteit, I., D. T. Pham, M. E. Gharamti, and X. Luo, 2015: Mitigating observation perturbation sampling errors in the stochastic EnKF. *Mon. Wea. Rev.*, **143**, 2918–2936, https://doi.org/10.1175/MWR-D-14-00088.1.

Hunt, B. R., and Coauthors, 2004: Four-dimensional ensemble Kalman filtering. *Tellus A: Dynamic Meteorology and Oceanography*, **56**(4), 273–277, https://doi.org/10.3402/tellusa.v56i4.14424.

Huo, Z. H., and W. S. Duan, 2019: The application of the orthogonal conditional nonlinear optimal perturbations method to typhoon track ensemble forecasts. *Science China Earth Sciences*, **62**, 376–388, https://doi.org/10.1007/s11430-018-9248-9.

Huo, Z. H., W. S. Duan, and F. F. Zhou, 2019: Ensemble forecasts of tropical cyclone track with orthogonal conditional nonlinear optimal perturbations. *Adv. Atmos. Sci.*, **36**, 231–247, https://doi.org/10.1007/s00376-018-8001-1.

Jiang, L., W. S. Duan, and H. L. Liu, 2022: The most sensitive initial error of sea surface height anomaly forecasts and its implication for target observations of mesoscale eddies. *J. Phys. Oceanogr.*, **52**, 723–740, https://doi.org/10.1175/JPO-D-21-0200.1.

Jiang, L., W. S. Duan, and H. Wang, 2024: The sensitive area for targeting observations of paired mesoscale eddies associated with sea surface height anomaly forecasts. *J. Geophys. Res.:*

Oceans, **129**, e2023JC020572, https://doi.org/10.1029/2023JC020572.

Jiang, Z. N., and M. Mu, 2009: A comparison study of the methods of conditional nonlinear optimal perturbations and singular vectors in ensemble prediction. *Adv. Atmos. Sci.*, **26**(3), 465–470, https://doi.org/10.1007/s00376-009-0465-6.

Leith, C. E., 1974: Theoretical skill of Monte Carlo forecasts. *Mon. Wea. Rev.*, **102**, 409–418, https://doi.org/10.1175/1520-0493(1974)102<0409:Tsomcf>2.0.Co;2.

Leon, S. J., Å. Björck, and W. Gander, 2013: O Gram-Schmidt orthogonalization: 100 years and more. *Numerical Linear Algebra with Applications*, **20**, 492–532, https://doi.org/10.1002/nla.1839.

Leutbecher, M., and T. N. Palmer, 2008: Ensemble forecasting. *J. Comput. Phys.*, **227**, 3515–3539, https://doi.org/10.1016/j.jcp.2007.02.014.

Li, H., E. Kalnay, and T. Miyoshi, 2009: Simultaneous estimation of covariance inflation and observation errors within an ensemble Kalman filter. *Quart. J. Roy. Meteor. Soc.*, **135**, 523–533, https://doi.org/10.1002/qj.371.

Liu, K., W. H. Guo, L. L. Da, J. Y. Liu, H. Q. Hu, and B. L. Cui, 2021: Improving the thermal structure predictions in the Yellow Sea by conducting targeted observations in the CNOP-identified sensitive areas. *Scientific Reports*, **11**, 19518, https://doi.org/10.1038/s41598-021-98994-7.

Liu, T., and Coauthors, 2023: A multi-model prediction system for ENSO. *Science China Earth Sciences*, **66**, 1231–1240, https://doi.org/10.1007/s11430-022-1094-0.

Lorenz, E. N., 1963: Deterministic nonperiodic flow. *J. Atmos. Sci.*, **20**(2), 130–141, https://doi.org/10.1175/1520-0469(1963)020<0130:DNF>2.0.CO;2.

Lorenz, E. N., 1996: Predictability: A problem partly solved. *Seminar on Predictability*. Shinfield Park, Reading, ECMWF, 1–18. [Available online from https://www.ecmwf.int/en/elibrary/75462-predictability-problem-partly-solved]

Lorenz, E. N., and K. A. Emanuel, 1998: Optimal sites for supplementary weather observations: Simulation with a small model. *J. Atmos. Sci.*, **55**(3), 399–414, https://doi.org/10.1175/1520-0469(1998)055<0399:OSFSWO>2.0.CO;2.

Mason, I. B., 1982: A model for assessment of weather forecasts. *Aust. Meteor. Mag.*, **30**, 291–303.

Molteni, F., R. Buizza, T. N. Palmer, and T. Petroliagis, 1996: The ECMWF ensemble prediction system: Methodology and validation. *Quart. J. Roy. Meteor. Soc.*, **122**(529), 73–119, https://doi.org/10.1002/qj.49712252905.

Mu, M., and Z. N. Jiang, 2008: A new approach to the generation of initial perturbations for ensemble prediction: Conditional nonlinear optimal perturbation. *Chinese Science Bulletin*, **53**, 2062–2068, https://doi.org/10.1007/s11434-008-0272-y.

Mu, M., W. S. Duan, and B. Wang, 2003: Conditional nonlinear optimal perturbation and its applications. *Nonlinear Processes in Geophysics*, **10**, 493–501, https://doi.org/10.5194/npg-10-493-2003.

Mu, M., W. S. Duan, and B. Wang, 2007: Season‐dependent dynamics of nonlinear optimal error growth and El Niño‐Southern Oscillation predictability in a theoretical model. *J. Geophys. Res.: Atmos.*, **112**, D10113, https://doi.org/10.1029/2005jd006981.

Mu, M., F. F. Zhou, and H. L. Wang, 2009: A method for identifying the sensitive areas in targeted Observations for tropical cyclone prediction: Conditional Nonlinear optimal perturbation. *Mon. Wea. Rev.*, **137**, 1623–1639, https://doi.org/10.1175/2008MWR2640.1.

Orrell, D., 2003: Model error and predictability over different timescales in the Lorenz '96 Systems. *J. Atmos. Sci.*, **60**, 2219–2228, https://doi.org/10.1175/1520-0469(2003)060<2219:MEAPOD>2.0.CO;2.

Peña, M., and Z. Toth, 2014: Estimation of analysis and forecast error variances. *Tellus A: Dynamic Meteorology and Oceanography*, **66**(1), 21767, https://doi.org/10.3402/tellusa.v66.21767.

Qin, X. H., W. S. Duan, P. W. Chan, B. Y. Chen, and K. N. Huang, 2023: Effects of dropsonde data in field campaigns on forecasts of tropical cyclones over the Western North Pacific in 2020 and the role of CNOP sensitivity. *Adv. Atmos. Sci.*, **40**, 791–803, https://doi.org/10.1007/s00376-022-2136-9.

Revelli, J. A., M. A. Rodríguez, and H. S. Wio, 2010: The use of rank histograms and MVL diagrams to characterize ensemble evolution in weather forecasting. *Adv. Atmos. Sci.*, **27**, 1425–1437, https://doi.org/10.1007/s00376-009-9153-6.

Rivière, O., G. Lapeyre, and O. Talagrand, 2008: Nonlinear generalization of singular vectors: Behavior in a baroclinic unstable flow. *J. Atmos. Sci.*, **65**, 1896–1911, https://doi.org/10.1175/2007JAS2378.1.

Talagrand, O., R. Vautard, and B. Strauss, 1997: Evaluation of probabilistic prediction systems. *Workshop on Predictability*, Shinfield Park, Reading, ECMWF, 1-25. https://www.ecmwf.int/en/elibrary/76596-evaluation-probabilistic-prediction-systems.

Terwisscha van Scheltinga, A. D., and H. A. Dijkstra, 2008: Conditional nonlinear optimal perturbations of the double-gyre ocean circulation. *Nonlinear Processes in Geophysics*, **15**, 727–734, https://doi.org/10.5194/npg-15-727-2008.

Toth, Z., and E. Kalnay, 1993: Ensemble forecasting at NMC: The generation of perturbations. *Bull. Amer. Meteor. Soc.*, **74**, 2317–2330, https://doi.org/10.1175/1520-0477(1993)074<2317:EFANTG>2.0.CO;2.

Toth, Z., and E. Kalnay, 1997: Ensemble forecasting at NCEP and the breeding method. *Mon. Wea. Rev.*, **125**, 3297–3319, https://doi.org/10.1175/1520-0493(1997)125<3297:EFANAT>2.0.CO;2.

Vannitsem, S., and Z. Toth, 2002: Short-term dynamics of model errors. *J. Atmos. Sci.*, **59**, 2594–2604, https://doi.org/10.1175/1520-0469(2002)059<2594:STDOME>2.0.CO;2.

Wang, Y., and W. S. Duan, 2019: Influences of initial perturbation amplitudes and ensemble sizes on the ensemble forecasts made by CNOPs method. *Chinese Journal of Atmospheric Sciences*, **43**(4), 915–929, https://doi.org/10.3878/j.issn.1006-9895.1810.18219. (in Chinese with English abstract)

Wei, M. Z., and Z. Toth, 2003: A new measure of ensemble performance: Perturbation versus error correlation analysis (PECA). *Mon. Wea. Rev.*, **131**, 1549–1565, https://doi.org/https://doi.org/10.1175//1520-0493(2003)131<1549:Anmoep>2.0.Co;2.

Whitaker, J. S., and T. M. Hamill, 2002: Ensemble data assimilation without perturbed observations. *Mon. Wea. Rev.*, **130**(7), 1913–1924, https://doi.org/10.1175/1520-0493(2002)130<1913:EDAWPO>2.0.CO;2.

Yamaguchi, M., and S. J. Majumdar, 2010: Using TIGGE data to diagnose initial perturbations and their growth for tropical cyclone ensemble forecasts. *Mon. Wea. Rev.*, **138**, 3634–3655, https://doi.org/10.1175/2010MWR3176.1.

Yang, L. C., W. S. Duan, and Z. F. Wang, 2023: An approach to refining the ground meteorological observation stations for improving $PM_{2.5}$ forecasts in Beijing-Tianjin-Hebei region. *Geoscientific Model Development*, **16**, 3827–3848, https://doi.org/10.5194/gmd-16-3827-2023.

Yang, L. C., W. S. Duan, Z. F. Wang, and W. Y. Yang, 2022: Toward targeted observations of the meteorological initial state for improving the $PM_{2.5}$ forecast of a heavy haze event that occurred in the Beijing-Tianjin-Hebei region. *Atmospheric Chemistry and Physics*, **22**, 11 429–11 453, https://doi.org/10.5194/acp-22-11429-2022.

Yoden, S., 2007: Atmospheric predictability. *J. Meteor. Soc. Japan*, **85B**, 77–102, https://doi.org/10.2151/jmsj.85B.77.

Zhang, H., W. S. Duan, and Y. C. Zhang, 2023a: Using the orthogonal conditional nonlinear optimal perturbations approach to address the uncertainties of tropical cyclone track forecasts generated by the WRF model. *Wea. Forecasting*, **38**, 1907–1933, https://doi.org/10.1175/WAF-D-22-0175.1.

Zhang, Y. C., W. S. Duan, S. Vannitsem, and H. Zhang, 2023b: A new approach to represent model uncertainty in the forecasting of tropical cyclones: The orthogonal nonlinear forcing singular vectors. *Quart. J. Roy. Meteor. Soc.*, **149**, 2206–2232, https://doi.org/10.1002/qj.4502.